

Research Paper

Thermal Performance Study of Plate-finned Vapor Chamber Heat Sink

Mohammed A. Al-Rahman¹, Saeed A.A. Ibrahim², M. Elfaisal Elrefaie¹

¹ Department of Mechanical Engineering, Al Azhar University, Cairo, Egypt, Email: mohammadabdoel-rahman.18@azhar.edu.eg (M.A.R.); m.abdo202084@gmail.com (M.E.E.)

² Department of Mechanical Engineering, Zagazig University, Zagazig, Egypt, Email: sabdi@zu.edu.eg

Received July 06 2023; Revised September 04 2023; Accepted for publication November 09 2023.

Corresponding author: M.A. Al-Rahman (mohammadabdoel-rahman.18@azhar.edu.eg)

© 2023 Published by Shahid Chamran University of Ahvaz

Abstract. This study focuses on improving the thermal characteristics of a plate-finned heat sink (PFHS) by incorporating a vapor chamber (VC) through experimental investigation. The research examines the influence of various parameters, including Reynolds number (Re), heat input, filling ratio (FR), and operating vacuum pressure, on the thermal performance of the VC. The results demonstrate that the utilization of a VC leads to a significantly more uniform temperature distribution along the base of the PFHS and low overall temperatures. Conversely, in the absence of a VC, the PFHS exhibits a non-uniform temperature distribution, with a bell-shaped profile and concentrated high temperatures at the center at the same operating conditions. The results indicate that an operating vacuum pressure of 1kPa produces the most favorable performance. Additionally, a filling ratio of 50% proves to be optimal across the range of heat inputs from 10 to 90 W.

Keywords: Heat sink, Vapor chamber, Thermal resistance, electronic devices cooling.

1. Introduction

The increasing advancement of electronic devices has led to a growing need for effective thermal control to prevent malfunctions caused by concentrated heat flux, commonly referred to as hotspots [1-3]. Efficient heat dissipation and thermal spreading within electronic devices have become significant challenges [4, 5]. Therefore, numerous methods have been introduced to enhance conventional heat transfer techniques. These methods include the utilization of vapor chambers [6, 7], microchannels [8], nanofluids [9], porous media [10], and modifications in geometries [11].

Vapor chambers, in particular, have gained significant attention as highly effective and efficient heat spreaders in various electronic devices [12-14] such as hard disk drivers [15], smartphones [16], LEDs [17-19], photovoltaic [20], solar collectors [21], and fuel cells [22-24]. A vapor chamber (VC) is a flat vacuum vessel made of copper or other materials. The VC contains a small quantity of liquid such as water or other liquid coolants. The vessel sides may be lined with wick structures or without wick structures [25]. The heat is generated by an electronic component such as a CPU in a laptop. The heat is transferred to the VC by conduction through thermal grease (commonly used as an interface material between heat sinks and the CPU) [26]. This heat causes the liquid inside the evaporator section to vaporize, creating a vapor that flows to the cooler condenser section. The vapor loses the heat at the condenser section and condenses back into liquid form. The condensed liquid then returns to the evaporator section by either capillary effect or gravity, creating a continuous cycle that effectively cools the electronic device.

There are many working studies to improve VC thermal performance and its fabrication. Wang and Vafai [27] experimentally investigated the thermal performance of copper flat heat pipe. The study found that the temperature distribution along the condenser wall surface was quite even. The highest thermal resistance in the VC was produced in the evaporator section, which influences the overall performance of the VC [28] evaluated the thermal performance of an aluminum VC heat sink, which used acetone as a working fluid and used micro stainless steel wick structures fabricated by the metal etch. The study found that a filling ratio of 30% yielded the best thermal performance. This performance improved as the heat load was increased. Hsieh et al. [29] experimentally investigate the heat spread of a copper VC without a wick. The distilled water is used as a working fluid. The results show that VCs are a better way to spread heat than traditional solid metal heat sinks under the same conditions. They also noted that the experimental study on VC heat sinks is very limited. Koito et al. [30] numerically investigated the thermal performance of the VC and validated the numerical analysis by experimental investigation. Ming et al. [31] experimentally studied the use of magnetic working fluid in a copper disk-shaped VC without a wick structure and compared the findings with those obtained using water. They found that the optimum charge ratio for the magnetic fluid was 53.5%. They suggest that magnetic fluid may be a promising alternative to traditional working fluids for VC. Also, Ming et al. [32] investigated the thermal behavior of a grooved VC using numerical and experimental methods. The results demonstrate that the grooved structure is capable of producing a capillary loop between the evaporation and condensation surfaces, thereby enhancing the heat transfer in the VC. Wang et al. [33] evaluated the thermal performance of a vapor chamber by a novel formula function in vapor chamber materials, working fluid, vapor chamber size, vacuum pressure, and height of working fluid inside the chamber. The results demonstrate that the thermal performance of



the vapor chamber increased with the size of the vapor chamber increased. Attia and El-Assal [34] experimentally investigated the thermal performance of a copper annular-shaped VC without a wick structure using different working fluids. The study found that the thermal performance of using water as a working fluid was much better than using methyl alcohol. The study also indicated that the optimum charge was 30% for most tested working fluids. Peng et al. [35] investigate the heat transfer of an aluminum VC without a wick structure experimentally. The study found that increasing the operating vacuum pressure improved thermal performance. Additionally, using acetone as the working fluid resulted in a thermal performance better compared to water. Naphon et al. [36] investigated the thermal performance of a copper VC. The effect of heat sink configurations, coolant flow direction types, filling ratios, and different working fluids on cooling efficiency are studied. Liu et al. [37] experimentally investigated the heat transfer characteristics of a wickless VC during condensation and evaporation. The study found that the thermal behavior increased as the power input increased, and the 33% filling ratio is the optimum for overall heat transfer performance. Though the work of Ladekar et al. [38], the heat transfer characteristics of a heat sink with VC were investigated numerically. In a VC utilizing acetone as the working fluid, the study shows that the thermal resistance of the integrated heat sink vapor chamber (IHSVC) decreased by 49.6% as the heater area increased by a factor of 1.25.

This review shows that the vapor chamber (VC) is one of the most effective methods for heat dissipation in electronic devices and the challenge to dissipate the generated heat from electronic devices properly and uniformly and overcome hotspots (local overheating) is an open topic despite valuable research efforts. This work investigates experimentally the thermal performance enhancement of a PFHS integrated with a new design of a wickless vapor chamber across a range of operating conditions. The effects of parameters including Reynolds number, heat input, vacuum pressure, and fill ratio are analyzed. This research contributes to the enhancement of heat dissipation in electronic devices, addressing the growing demand for efficient thermal control.

2. Experimental Setup

Figure 1 presents a schematic of the experimental setup that was used to study the thermal performance of the PFHS with and without VC. The setup consists of the following:

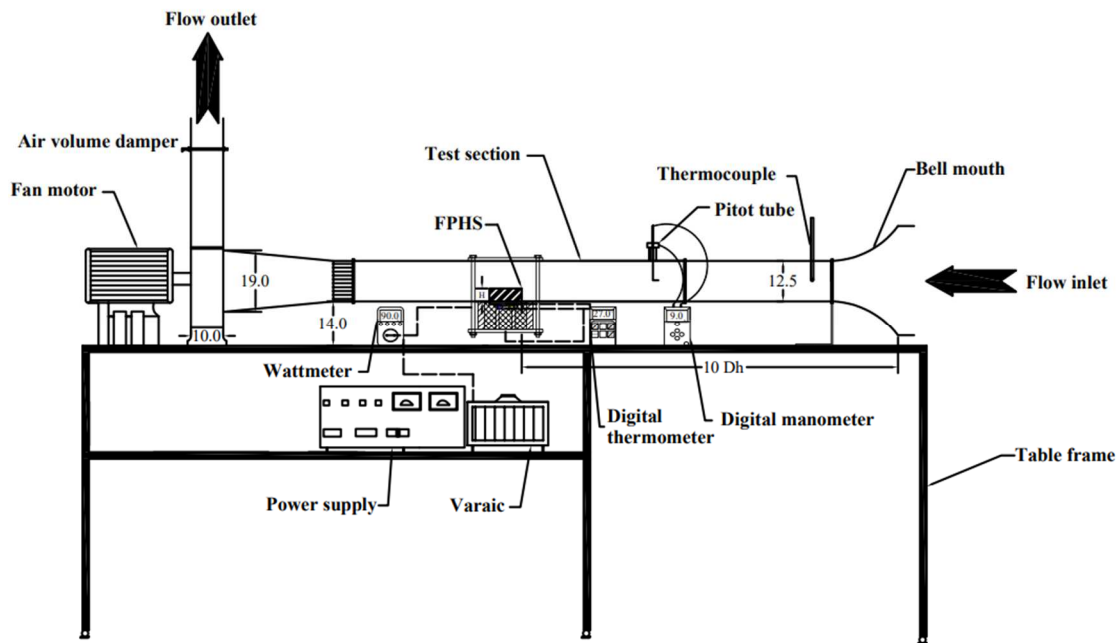


Fig. 1. A schematic configuration of the experimental setup.

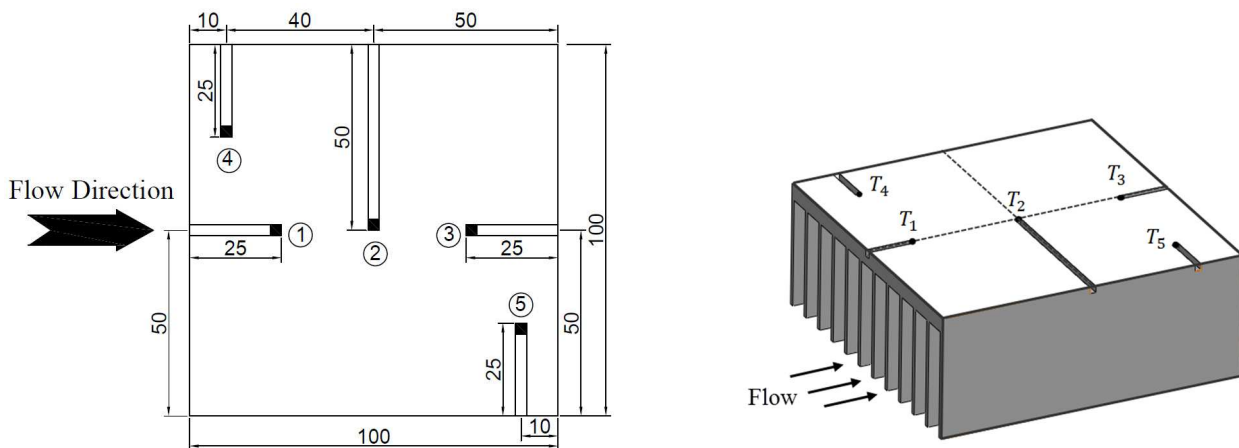


Fig. 2. PFHS configuration and thermocouple's location.



2.1. Test Section

A test section consists of a main duct fabricated from a 6-mm thick Plexiglas plate and assembled correctly to prevent air leakage. The test section has dimensions of 1000 mm in length and a cross-section (125 mm x 125 mm). The air is drawn by a centrifugal fan coupled with a 1 hp electric motor. The air enters the test section through a bell mouth. The purpose of the bell mouth inlet is to ensure a smooth and uniform flow of air into the test section. The plate-finned heat sink was installed after 10 hydraulic diameters (D_h) of the test section from the bell mouth inlet, where the hydrodynamic entry length in turbulent flow is equal to $10 D_h$ [39].

2.2. Plate Finned- Heat Sink (PFHS)

The PFHS is fabricated from aluminum alloy 2017. The PFHS has a base area of 100 mm x 100 mm, and base thickness (t_b) = 5 mm. Its fins have a height of (H) = 35 mm, and a thickness of (t) = 1.5 mm. Three PFHS with different numbers of fins ($N = 8$, $N = 12$, and $N = 16$) are studied. The heat sink base has five T-Type (copper-constantan) thermocouples installed to measure the temperatures as shown in Fig. 2.

2.3. Vapor Chamber (VC)

A wickless VC was constructed and designed as illustrated in Fig. 3. The tested VC comprises two main parts: the chamber, and the top plate. The chamber and top plate were held together by circumferential bolts. To prevent leakage, a suitable O-ring was used. The five columns built in the chamber have the same chamber height (3.5mm height) to prevent deflection in the top plate during the vacuum. The VC is made from copper and has outer dimensions of 100 mm x 100 mm x 6 mm and inner dimensions of 80 mm x 80 mm x 3.5 mm. The charging valve was used to charge working fluid easily. To ensure the (VC) is sealed properly, a leakage test is performed. An air compressor pressurizes the VC to approximately 1.5 bar gauge pressure. The VC is then submerged in a water bath to check for any escaping air bubbles that would indicate a leak. Once no leaks are detected, the VC is prepared to charge with working fluid (distilled water).

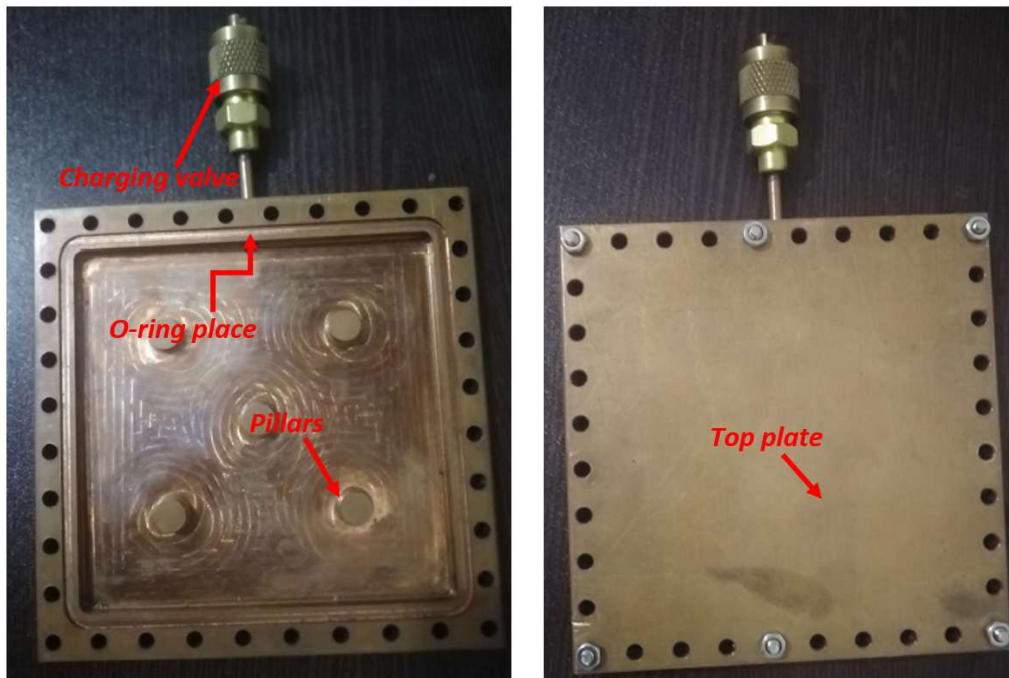


Fig. 3. Photos of the VC Configuration.

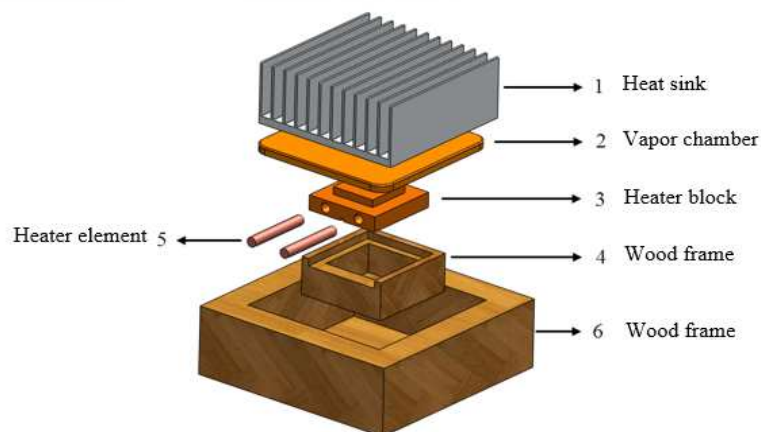


Fig. 4. The PFHS with VC and heating source assembly.



Table 1. The range of parameters in the study.

Parameter	Value	Unit
heat input range(Q)	10 - 90	W
Number of Fins (N)	8 - 16	
Flow Re	15,580 - 62,310	
VC. filling ratio (FR)	10 - 70	%
VC. working fluid	Distilled water	
VC. operating pressure	1 - 10	kPa

2.4. Heat Source

The Heating source comprises a heater block and two electric pencil heaters with a power output of 60 W each. The heater block is made from copper with dimensions of 30mm x 30mm x 5mm at the top and 50mm x 50mm x 10mm at the base of the heater. To maintain a constant heat flux, a variable AC power supply (Variaic) is utilized to control the electrical voltage, current, and power input to the heater elements. The digital wattmeter is used to measure power input (P_{input}) to the heater elements. The heating source is placed inside a wooden frame and insulated by glass wool, which has a thermal conductivity of ($k = 0.023$ W/m.K) to minimize heat losses. The assembly of the heater block and heater elements with the PFHS with VC is illustrated in Fig. 4.

2.5. Charging Process

The charging unit consists of several components: a vacuum pump, valves, an injector (syringe), and a pressure gauge, as shown in Fig. 5. To begin the suction process, follow these steps: close all valves initially, start the vacuum pump, then sequentially open valves numbered (1), (2), and (4) to create a vacuum within the VC until reaching the desired operating vacuum pressure. Afterward, close valves (4), (2), and (1) in the same order, and turn off the vacuum pump. Disconnect the VC from the suction unit to weigh the empty VC using a digital weighing scale with a readability of 0.01 g (Chyo-petit balance). Reconnect the VC to the charging unit to fill it with distilled water, adhering to the specified filling ratio. Open valves numbered (3) and (4) to allow the entry of distilled water into the VC, naturally by the pressure difference between the VC and the syringe. Re-weigh the VC to verify that the correct amount of distilled water has been charged. The preparation of the required quantity of distilled water involves the following steps: Begin by weighing the empty injector (syringe), then proceed to fill the syringe with the corresponding volume of distilled water according to the filling ratio. Subsequently, weigh the syringe containing the distilled water to determine its weight. Finally, charge the VC with the appropriate filling ratio and position it on the evaporator side of the heating source, while placing the heat sink on the condenser side. To further enhance heat transfer, apply a thin layer of thermal paste with a thermal conductivity of $K = 1.9$ W/m.K between the VC and the heat sink, as well as between the VC and the heater.

3. Experimental Procedure

Initially, the thermal performance of the PFHS was investigated without VC. The PFHS which has the best thermal performance was mounted on a VC to investigate the thermal criteria of VC. A sequence of tests was then conducted under different conditions as shown in Table 1.

3.1. Data Reduction

The air velocities in the wind tunnel were measured by a digital differential pressure manometer (Model: HD755, with range ± 350 mm H₂O, and accuracy $\pm 0.01\%$ mm H₂O) using a pitot tube at the entrance of the test section. The air velocity was controlled by an air volume damper located at the wind tunnel outlet. The temperatures were measured at a steady state condition by a digital thermometer (Model: OMEGA: HH21A, with range 0:400°C of type T, and accuracy $\pm 0.1\% + 0.6$ °C) using several thermocouple type T located at the wind tunnel inlet, PFHS base, top and bottom of the heater and bottom of the insulation to measure the air temperature T_a , the temperature distribution on PFHS base (T1, T2, T3, T4, and T5), upper and lower temperature of the heater (T_{h-up} and T_{ins-up}) and insulation temperature ($T_{ins-down}$) respectively. The input electric power to the heater (P_{input}) was measured by a wattmeter device (Model: UT230B-EU, with range 0-3680 W, and accuracy $\pm 1\%$) and adjusted via a variac. As shown in Fig. 6, the heat loss from the heating source to the surrounding (Q_{loss}) through the insulation can be estimated by Eq. (1):

$$Q_{Loss} = K_{ins} A_{ins} \frac{T_{in-up} - T_{ins-down}}{H_{ins}} \quad (1)$$

where K_{ins} is the insulation's thermal conductivity and A_{ins} cross-section area of the insulation and H_{ins} the height of the insulation. Therefore, the heat input (Q) can be obtained by Eq. (2):

$$Q = P_{input} - Q_{loss} \quad (2)$$

where P_{input} is the power measured by a digital wattmeter.

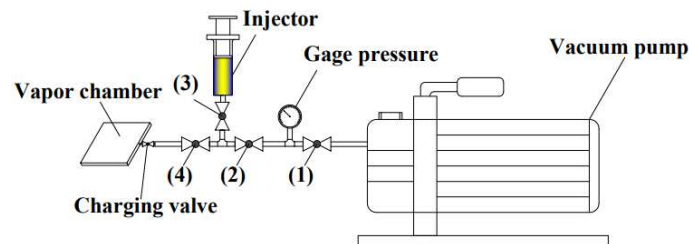


Fig. 5. Schematic of the charging unit components.



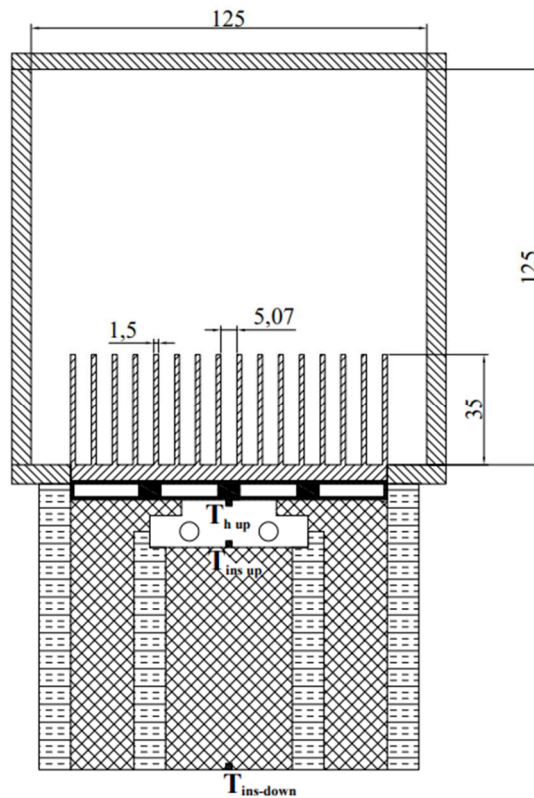


Fig. 6. A cross-section in wind tunnel.

The thermal resistance of PFHS ($R_{th HS}$) is determined by Eq. (3):

$$R_{th HS} = \frac{T_{b-avg} - T_a}{Q} \tag{3}$$

where $T_{b-avg} = (\sum_{i=1}^{i=5} T_i) / 5$. Also, the thermal resistance of VC ($R_{th VC}$) is determined by Eq. (4):

$$R_{th VC} = \frac{T_{h-up} - T_{b-avg}}{Q} \tag{4}$$

Reynolds number (Re) calculated by Eq. (5):

$$Re = \frac{\rho_a U_a D_h}{\mu_a} \tag{5}$$

where, ρ_a is the air density, U_a is the airflow velocity ($U_a = 2 \text{ m/s} : 8 \text{ m/s}$), D_h is the hydraulic diameter of the wind tunnel estimated by $D_h = 4A / P$, and μ_a is the dynamic viscosity of air. The Nusselt number (Nu_{Dh}) of the heat sink is estimated by Eq. (6):

$$Nu_{Dh} = \frac{h D_h}{K_f} \tag{6}$$

where K_f is the thermal conductive of the air and estimated at $T_{mean} = (T_{b-avg} + T_a) / 2$ and h is the heat transfer coefficient estimated by Eq. (7):

$$h = \frac{Q}{A_{Conv.}(T_{b-avg} - T_a)} = \frac{1}{A_{Conv.} R_{th}} \tag{7}$$

where $A_{Conv.}$ is the convective area of the heat sink. The convective area depends on the design and geometry of the heat sink. The filling ratio FR is obtained by Eq. (8):

$$FR = \frac{V_{wf}}{V_{VC}} * 100\% \tag{8}$$

where V_{wf} is the volume of the measured working fluid, and V_{VC} is the inner volume of the vapor chamber.

3.2. Uncertainty Analysis

In the current study, uncertainty analysis was performed, and the total uncertainty in derived parameter F was calculated using the following Eq. (9) [40]:



$$\omega_F = \sqrt{\left(\left(\frac{\partial F}{\partial x_1}\right)^2 \omega_{x_1}^2 + \left(\frac{\partial F}{\partial x_2}\right)^2 \omega_{x_2}^2 + \dots + \left(\frac{\partial F}{\partial x_n}\right)^2 \omega_{x_n}^2\right)} \tag{9}$$

where ω_F is the uncertainty of the variable F , ω_{x_1} is the uncertainty of parameter x_1 , and $\partial F/\partial x_1$ is the partial derivative of F concerning x_1 . The measurement uncertainty and accuracy are calculated using the uncertainty of primary measurements. The convective heat transfer coefficient of a heat sink is determined by heat load and temperature measurements. The reading uncertainty of T-type thermocouples is $\pm 0.6^\circ\text{C}$ and the wattmeter has an accuracy of $\pm 1\%$. Substituted in the uncertainty formula Eq. (9), the uncertainty of the convective heat transfer coefficient accounted for $\pm 1.03\%$. Similarly, the thermal resistance and Nusselt number accounted for $\pm 1.03\%$ uncertainty in the uncertainty analysis.

4. Results and Discussion

4.1. Plat Finned-Heat Sink without Vapor Chamber

4.1.1. Thermal resistance of PFHS ($R_{th\ HS}$)

Figure 7 shows the effect of the Reynolds number on the thermal resistance of PFHS at various fins numbers ($N = 8, N = 12,$ and $N = 16$) and heat input $Q = 30\text{W}$. It is clear that as the Re increases, the thermal resistance of PFHS decreases, but the rate of decrease is greater at low Re than at high Re , this is because as Re increases the convective heat transfer coefficient increases therefore thermal resistance decreases. Additionally, the thermal resistance of PFHS also decreases as the fin number increases. This is because the PFHS surface area increases as the fins number (N) increases, therefore reducing the thermal resistance.

Based on the three well-known fluid mechanics governing equations, a numerical exercise was applied to the test section at different locations (Locations A and B as shown in Fig. 8). The numerical results at two locations are compared as shown in Fig. 9. The percentage deviation ($D = (R_{th@A} - R_{th@B}) / (R_{th@A}) \times 100$) between the numerical results at the two locations is less than 4.5%. That difference is attributed to the boundary layer effect.

4.1.2. Temperature distribution

Temperature distribution of the PFHS base at a different fins number, $Q = 30\text{ W}$ and $Re = 31,160$ is shown in Fig. 10, where X is the position of the thermocouple on the PFHS base and (L) is the length of PFHS, due to the smaller area of the heater compared to the base of the heat sink, as well as the relatively low value of the thermal conductivity of the heat sink. This leads to, the temperature distribution on the heat sink taking on a bell-shaped form. The temperature is a maximum at the middle of the base and decreases towards the edges. The maximum temperature value of the heat sink base decreases as the fins number increases.

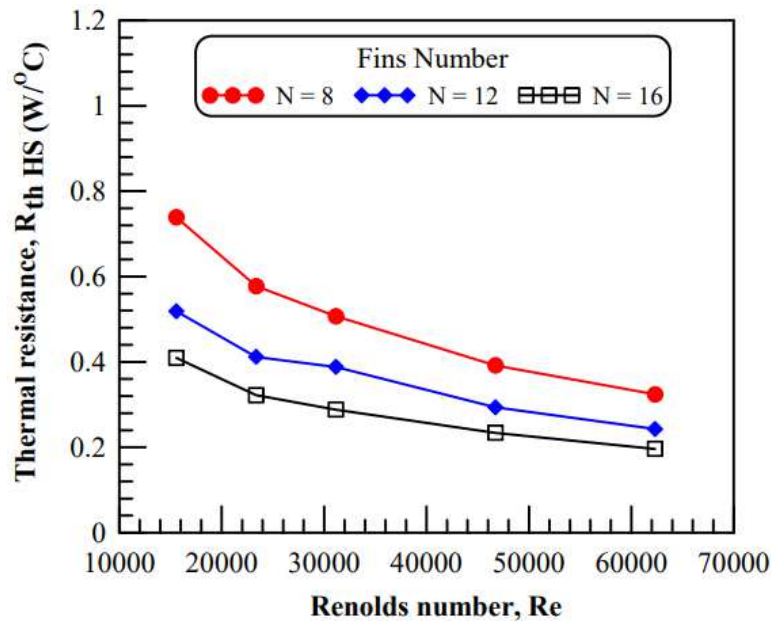


Fig. 7. Effect of Re on the thermal resistance of plate finned heat sink, $R_{th\ HS}$ at various fins numbers.

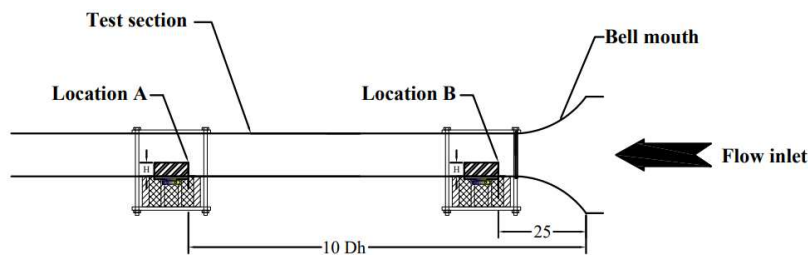


Fig. 8. The different locations of the test section.



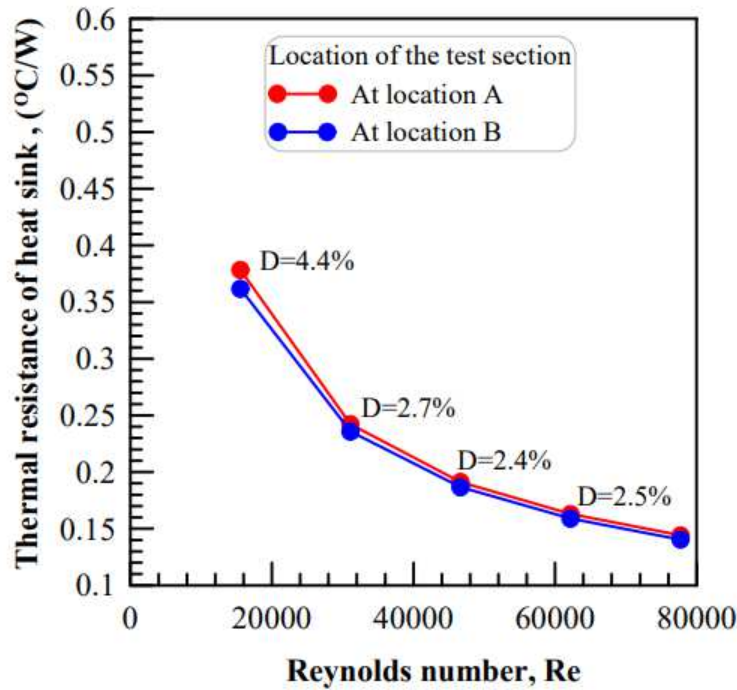


Fig. 9. CFD findings for the effect of test section location in the wind tunnel [41].

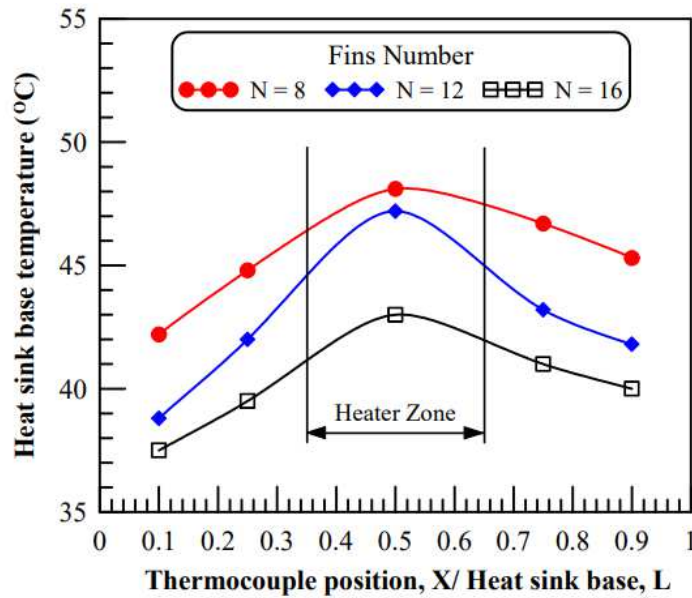


Fig. 10. Temperature distributions of the plat finned heat sink base.

4.2. Plat Finned Heat Sink with Vapor Chamber

Based on the previous results, the PFHS which has a fins number $N = 16$ has better thermal performance than the others, thus it was used with the VC.

4.2.1. Vapor chamber transient behavior

Figure 11 shows, the transient behavior of the experimental heater temperature (i.e., the temperature of the VC base) at different heat inputs and constant $Re = 31,160$. It is indicated that the time consumed to reach steady state conditions (i.e., the transient region) varied with heat inputs. As heat input is low, reaches a steady state faster than high heat input. The transient time for almost all heat inputs was approximately 1000 seconds.

4.2.2. Effect of heat input (Q)

Figure 12 depicts the effect of heat input on the thermal behavior of VC at various filling ratios and constant $Re = 31,160$. For all ranges of filling ratio, the thermal resistance of VC ($R_{th,vc}$) decreases as heat input increases and vice versa. This is maybe because, at low heat inputs, the heat is enough to boil or evaporate the distilled water, therefore the heat is transferred from the heater to the heat sink by conduction mode. With increasing heat input, the temperature of the heater increases as shown in Fig. 13, and the evaporation or the boiling of working fluid starts, and thermal resistance reduces.



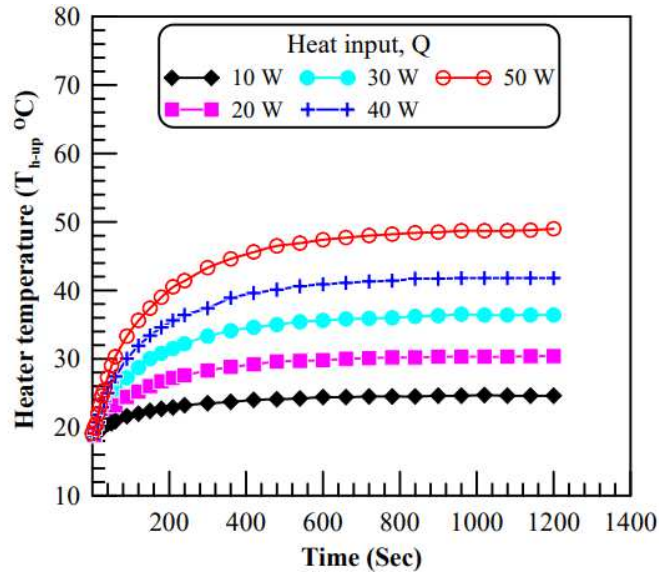


Fig. 11. Transient response of heater temperature.

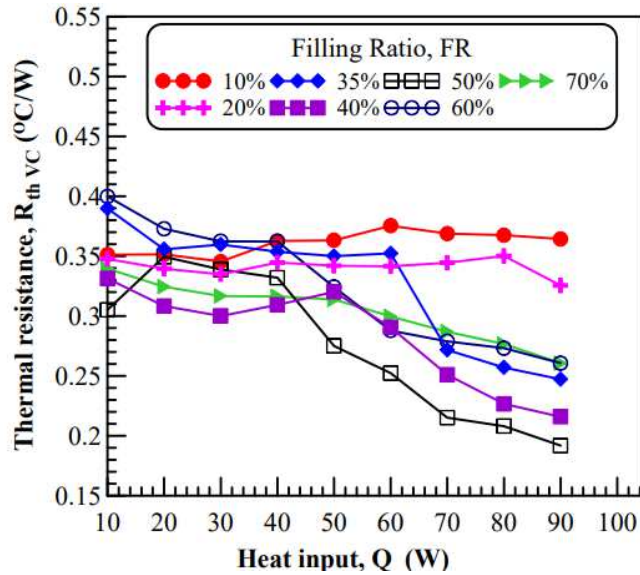


Fig. 12. The heat input effect on the thermal resistance of VC at various filling ratios (F.R.).

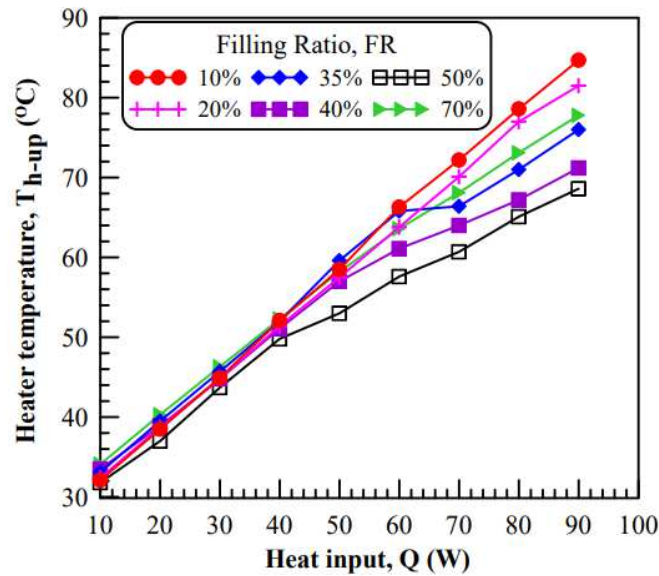


Fig. 13. The heat input affects heater temperature at various filling ratios (F.R.).



4.2.3. Effect of filling ratio (FR)

The effect of the filling ratio (FR) on the thermal performance of VC at $Re = 31,160$ and different heat inputs is shown in Fig. 14. The thermal resistance of VC decreases sharply as the filling ratio increases up to $FR = 50\%$. For the FR greater than 50% , the $R_{th, VC}$ increases as filling ratio increase as shown in Fig. 14(a). The effect of FR on the temperature of the heater (T_{h-up}) has the same trend. As shown in Fig. 14(b) the T_{h-up} increases as the filling ratio increases up to $FR = 50\%$. For FR greater than 50% , the T_{h-up} increases as the filling ratio increases. Figure 15 shows the effect of the filling ratio on temperature in the y-direction of the test section at constant heat input $Q = 90\text{ W}$ and constant $Re = 31,160$. The Filling ratio = 50% has a minimum temperature. According to this result, for this VC, the optimal filling ratio over the range of heat input is $FR = 50\%$. At the filling ratio is less than 50% , the amount of working fluid in the VC may be not enough to transfer the heat from the evaporator section to the condenser section and this may lead to dry out. While at a filling ratio greater than 50% , the amount of working fluid in the VC may be excess, and the thickness of working fluid at the evaporator section increase and increase the thermal resistance $R_{th, VC}$.

4.2.4. The effect of the operating vacuum pressure

The impact of the operating vacuum pressures on the temperature of the heater at $FR = 50\%$, $Re = 31,160$ and different heat inputs are shown in Fig. 16. The results indicate that the heater temperature with operating vacuum pressure = 1 kPa is lower than the heater temperature at other operating vacuum pressure, this may be due to the amount of residual air (no condensable gas) in the chamber is decreased with high the vacuum, therefore, decreasing the condensation and the boiling resistance and improving the heat transfer rate.

4.2.5. Effect of Reynolds number Re

By analyzing the VC's thermal performance, it was discovered that its optimal operating conditions are a 50% filling ratio and a 90 W heat input. Thus, it was essential to investigate the Reynolds number (Re) effect on the thermal performance of VC under optimum operating conditions. This is depicted in Fig. 17. The temperature of the heater decreases with an increase in the Reynolds number, and therefore the heat transfer rate via the VC will be faster, which will reduce the temperature of the heater, which is the desired goal of the study.

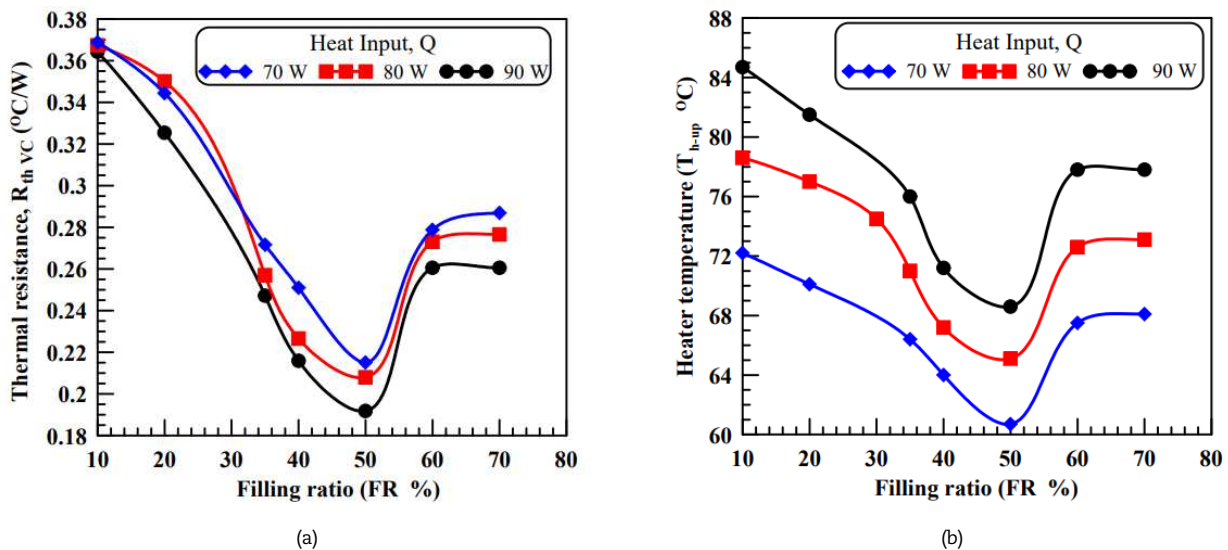


Fig. 14. Effect of the filling ratio on the thermal performance of VC: (a) Thermal resistance of VC ($R_{th, VC}$) (b) Heater temperature (T_{h-up}).

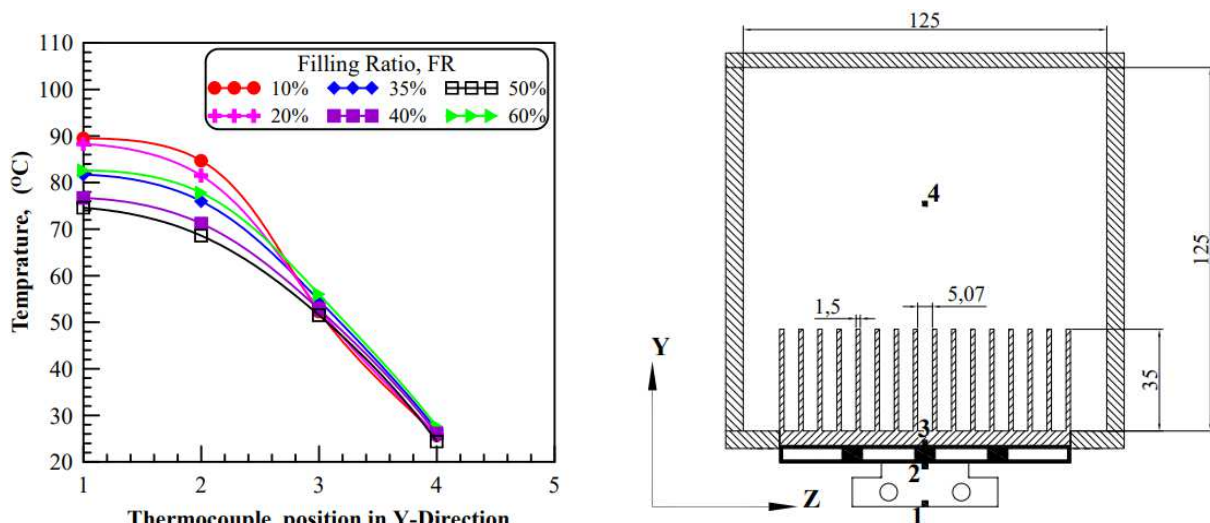


Fig. 15. Effect of the filling ratio on the temperature in the Y-Direction of the test section.



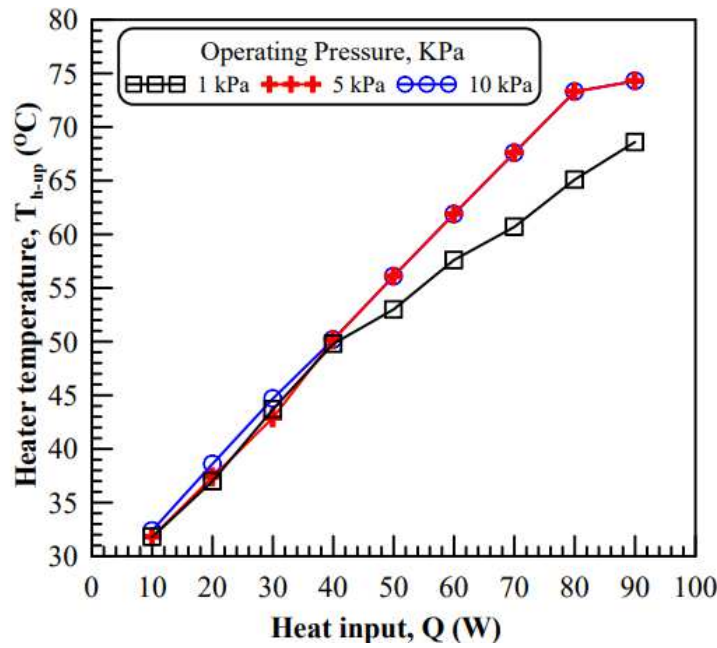


Fig. 16. The operating pressure affects the heater temperature.

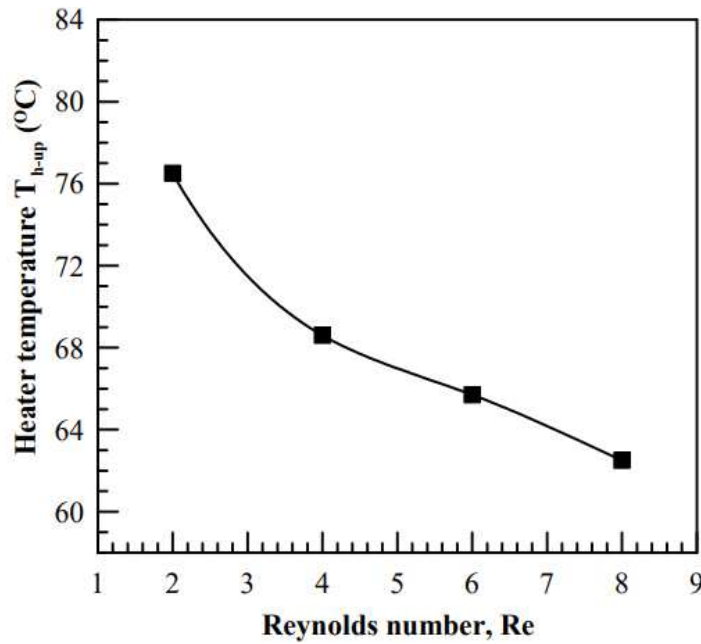


Fig. 17. The Effect of Re on the heater temperature.

4.2.6. Temperature distribution

Figure 18(a) shows a comparison of the temperature distribution along the center line of the PFHS base centerline with and without VC at fins number $N = 16$, heat input $Q = 30$ W, and $Re = 31,160$. With the use of VC, uniform temperature distribution and reduced overall temperatures are obtained along the PFHS base. This is because thermal spreading resistance decreases due to a phase change occurring in the VC, heat can be removed rapidly, and a local high temperature is avoided. Without VC, non-uniform temperature distribution and the bell-shaped with local high temperature at the center are obtained along the PFHS base. Electronic devices can be damaged by local high temperatures. Figure 18(b) shows the temperature distribution of the PFHS base with various heat inputs. The temperature line maintains its form and the temperature difference between the center and edges remains below 3 °C even with an increase in heat input up to 90 W. This means that the VC is more reliable for cooling electronic devices with high heat flux.

4.2.7. Nusselt number (Nu_{Dh})

Figure 19 shows a comparison Nu_{Dh} of PFHS with and without VC at constant heat input $Q = 30$ W, $FR = 50\%$, fins number $N = 16$, and different Re . It was clear that Nu_{Dh} is increasing as Re increases. Because as Re increase the heat transfer coefficient increase therefore Nusselt number increase.



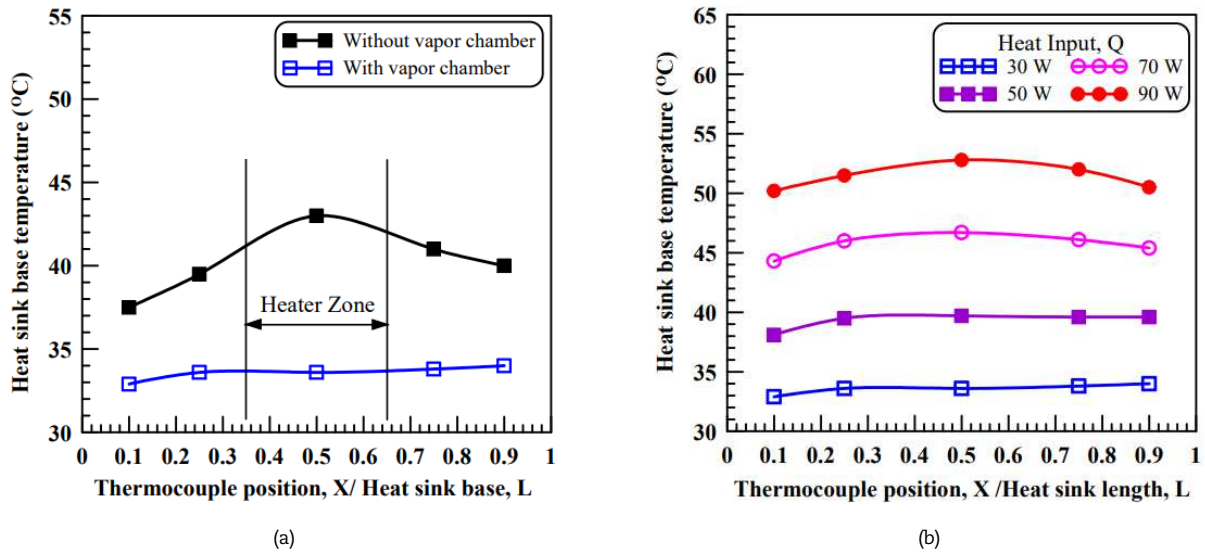


Fig. 18. The temperature distribution of PFHS base: (a) With and without VC at heat input, $Q = 30$ W, (b) With VC at different heat inputs.

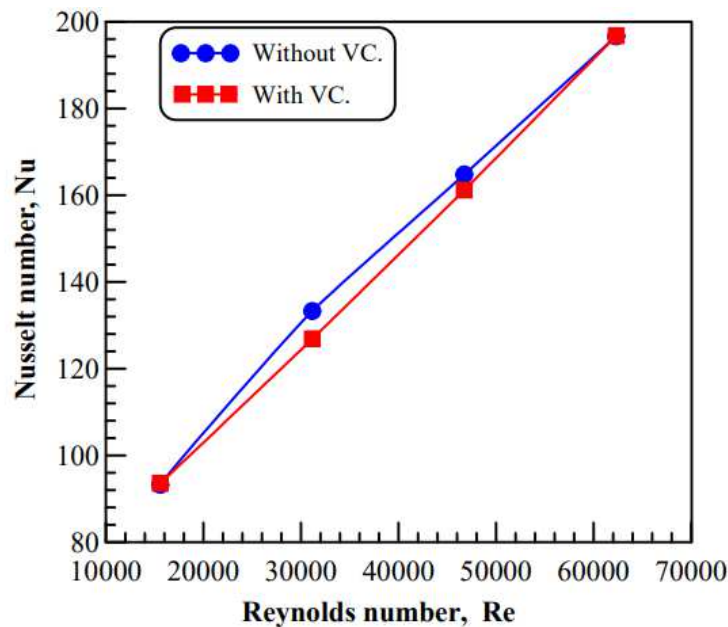


Fig. 19. Effect of Re on Nusselt number with using vapor chamber and without.

5. Conclusion

In this study, the thermal performance of PFHS with and without VC was investigated experimentally. The effects of different factors such as fins number, heat input (Q), filling ratio (FR), Reynolds number (Re), and operating pressure were presented and discussed. The main results of this study are as follows:

The thermal resistance of PFHS decreases as the fins number of PFHS, and Re increase. The thermal performance of PFHS increases as Re increases for both PFHS with and without VC. The thermal resistance of PFHS with VC decreases as the heat input increases, thus the VC is more effective in high heat input. The temperature of the PFHS base with a VC is more uniform compared with the temperature of the PFHS base without a VC. Therefore, a VC is more effective for spreading the concentrated heat flux. For this VC, the optimum filling ratio is 50%. The lowest heater temperature and the lowest thermal resistance at all heat inputs. Where the heater temperature = 68.6 °C and thermal resistance = 0.19 °C/W at the filling ratio = 50%. The heater temperature and thermal resistance decrease as the operating vacuum pressure increases in the test pressure range. For this VC, 1 kPa seems to be the optimum working pressure.

Author Contributions

Mohammed A. Al-Rahman conducted the experiments, analyzed the results, and prepared the original manuscript draft. Saeed A.A. Ibrahim has contributed to the experimental technical work and provided some interpretation of the experimental results. M. Elfaisal Elrefaie developed, followed up, reviewed, and supervised the work and editing. All authors shared the manuscript writing and discussed the results, reviewed, and approved the final version of the manuscript.



Acknowledgments

The authors would like to thank Prof. Sayed Ahmed for his sincere help and invaluable discussion during the implementation of the present experimental work.

Conflict of Interest

The authors declared no potential conflicts of interest concerning the research, authorship, and publication of this article.

Funding

The authors received no financial support for the research, authorship, and publication of this article.

Data Availability Statements

The datasets generated and/or analyzed during the current study are available from the corresponding author on reasonable request.

Nomenclature

A	The cross-sectional area[m ²]	T	Temperature [°C]
FR	Filling Ratio [%]	U	Velocity [m/s]
H	Height [m]		
K	Thermal conductivity [W/m.K]	Subscript	
Nu	Nusselt number	a	air
P	Perimeter [m]	avg.	average
P _{input}	Power input [W]	HS	heat sink
Q	Heat load [W]	Ins-up	insulation up
Re	Reynolds number	Ins-down	insulation down
R _{th}	Thermal resistance [°C/W]	VC	vapor chamber

References

- [1] Wu, G., Luo, Y., Bai, P., Wang, H., Cai, R., Tang, Y., Chen, X., Zhou, G., Modeling and experimental analysis of an internally cooled vapor chamber, *Energy Conversion and Management*, 235, 2021, 114017.
- [2] Liu, T., Yan, W., Yang, X., Wang, Sh., Improving the thermal performance of thin vapor chamber by optimizing screen mesh wick structure, *Thermal Science and Engineering Progress*, 36, 2022, 101535.
- [3] Bulut, M., Kandlikar, S.G., Sozbir, N., A Review of Vapor Chambers, *Heat Transfer Engineering*, 40, 2019, 1551-1573.
- [4] Dhaiban, H.T., Hussein, M.A., The Optimal Design of Heat Sinks: A Review, *Journal of Applied and Computational Mechanics*, 6(4), 2020, 1030-1043.
- [5] Mahmoudi J., CFD Analyses and Comparison of the Effect of Industrial Heat Sinks in Subsea Control System (SCS), *Journal of Applied and Computational Mechanics*, 9(1), 2023, 95-112.
- [6] Hassan, H., Harmand, S., A Three-Dimensional Study of Electronic Component Cooling Using a Flat Heat Pipe, *Heat Transfer Engineering*, 34, 2013, 596-607.
- [7] Lia, B., Huang, K., Yan, Y., Lic, Y., Twahaa, S., Zhua, J., Heat transfer enhancement of a modularised thermoelectric power generator for passenger vehicles, *Applied Energy*, 205, 2017, 868-879.
- [8] Khodabandeh, E., Rozati, S.A., Joshaghani, M., Akbari, O.A., Akbari, S., Toghraie, D., Thermal performance improvement in water nanofluid/GNP-SDBS in novel design of double-layer microchannel heat sink with sinusoidal cavities and rectangular ribs, *Journal of Thermal Analysis and Calorimetry*, 136, 2019, 1333-1345.
- [9] Toghraie, D., Mashayekhi, R., Arasteh, H., Sheykhi, S., Niknejadi, M., Chamkha, A.J., Two-phase investigation of water-Al₂O₃ nanofluid in a micro concentric annulus under non-uniform heat flux boundary conditions, *International Journal of Numerical Methods for Heat & Fluid Flow*, 30(4), 2020, 1795-1814.
- [10] Arasteh, H., Mashayekhi R., Ghaneifar, M., Toghraie, D., Afrand, M., Heat transfer enhancement in a counter-flow sinusoidal parallel-plate heat exchanger partially filled with porous media using metal foam in the channels' divergent sections, *Journal of Thermal Analysis and Calorimetry*, 141, 2020, 1669-1685.
- [11] Arasteh, H., Mashayekhi, R., Goodarzi, M., Motaharpour, S.H., Dahari, M., Toghraie, D., Heat and fluid flow analysis of metal foam embedded in a doublelayered sinusoidal heat sink under local thermal non-equilibrium condition using nanofluid, *Journal of Thermal Analysis and Calorimetry*, 138, 2019, 1461-1476.
- [12] Li, Y., Hu, H., Li, C., Zhang, Y., Yang, S., Pan, M., Experimental investigation on enhanced flow and heat transfer performance of micro-jet impingement vapor chamber for high power electronics, *International Journal of Thermal Sciences*, 173, 2022, 107380.
- [13] Wang, R.-T., Wang, J.-C., Chang, T.-L., Experimental analysis for thermal performance of a vapor chamber applied to high-performance servers, *Journal of Marine Science and Technology*, 19, 2011, 353-360.
- [14] Zeng, J., Zhang, S., Chen, G., Lin, L., Sun, Y., Chuai, L., Yuan, W., Experimental investigation on thermal performance of aluminum vapor chamber using micro-grooved wick with reentrant cavity array, *Applied Thermal Engineering*, 130, 2018, 185-194.
- [15] Naphon, P., Wongwises, S., Wiriyaart, S., Application of two-phase vapor chamber technique for hard disk drive cooling of PCs, *International Communications in Heat and Mass Transfer*, 40, 2013, 32-35.
- [16] Zhou, W., Li, Y., Chen, Z., Deng, L., Gan, Y., Ultra-thin flattened heat pipe with a novel band-shape spiral woven mesh wick for cooling smartphones, *International Journal of Heat and Mass Transfer*, 146, 2020, 118792.
- [17] Huang, H.-S., Chiang, Y.-C., Huang, C.-K., Chen, S.-L., Experimental Investigation of Vapor Chamber Module Applied to High-Power Light-Emitting Diodes, *Experimental Heat Transfer*, 22, 2009, 26-38.
- [18] Wang, J.-C., Thermal Investigations on LED vapor chamber-based plates, *International Communications in Heat and Mass Transfer*, 38, 2011, 1206-1212.
- [19] Lu, Z., Huang, P.F.B., Henzen, A., Coehoorn, R., Liao, H., Zhou, G.F., Experimental investigation on the thermal performance of three-dimensional vapor chamber for LED automotive headlamps, *Applied Thermal Engineering*, 157, 2019, 113478.
- [20] Jouhara, H., Milko, J., Danielewicz, J., Sayegh, M.A., Szulgowska-Zgrzywa, M., Ramos, J.B., Lester, S.P., The performance of a novel flat heat pipe based thermal and PV/T (photovoltaic and thermal systems) solar collector that can be used as an energy-active building envelope material, *Energy*, 108, 2016, 148-154.
- [21] Wang, Z.-Y., Diao, Y.-H., Zhao, Y.-H., Wei, X.-Q., Chen, C.-Q., Wang, T.-Y., Liang, L., Compound parabolic concentrator solar air collection-storage system based on micro-heat pipe arrays, *Solar Energy*, 207, 2020, 743-758.
- [22] Tetuko, A.P., Shabani, B., Andrews, J., Thermal coupling of PEM fuel cell and metal hydride hydrogen storage using heat pipes, *International Journal of Hydrogen Energy*, 41, 2016, 4264-4277.
- [23] Huang, B., Jian, Q.F., Luo, L.Z., Bai, X.Y., Research on the in-plane temperature distribution in a PEMFC stack integrated with flat-plate heat pipe



- under different startup strategies and inclination angles, *Applied Thermal Engineering*, 179, 2020, 115741.
- [24] Li, Y.Y., Chang, G.F., Xu, Y.M., Zhang, J.N., Zhao, W., A Review of MHP Technology and Its Research Status in Cooling of Li-Ion Power Battery and PEMFC, *Energy & Fuel*, 34, 2020, 13335–13349.
- [25] Srimuang, W., Limkaisang, V., A correlation to predict the heat flux on the air-side of a vapor chamber with overturn-U flattened tubes, *Heat and Mass Transfer*, 52, 2016, 1683–1692.
- [26] Wiriyasart, S., Naphon, P., Thermal performance enhancement of vapor chamber by coating mini-channel heat sink with porous sintering media, *International Journal of Heat and Mass Transfer*, 126, 2018, 116–122.
- [27] Wang, Y., Vafai, K., An experimental investigation of the thermal performance of an asymmetrical flat plate heat pipe, *International Journal of Heat and Mass Transfer*, 43, 2000, 2657–2668.
- [28] Go, J.S., Quantitative thermal performance evaluation of a cost-effective vapor chamber heat sink containing a metal-etched micro wick structure for advanced microprocessor cooling, *Sensor and Actuators A: Physical*, 121, 2005, 549–556.
- [29] Hsieh, S.S., Lee, R.Y., Shyu, J.C., Chen, S.W., Thermal performance of flat vapor chamber heat spreader, *Energy Conversion and Management*, 49, 2008, 1774–1784.
- [30] Koito, Y., Imura, H., Mochizuki, M., Saito, Y., Torii, S., Numerical analysis and experimental verification on thermal fluid phenomena in a vapor chamber, *Applied Thermal Engineering*, 26, 2006, 1669–76.
- [31] Ming, Z., Zhongliang, L., Guoyuan, M., Shuiyuan, C., The experimental study on flat plate heat pipe of magnetic working fluid, *Experimental Thermal and Fluid Science*, 33, 2009, 1100–1105.
- [32] Ming, Z., Zhongliang, L., Guoyuan, M., The experimental and numerical investigation of a grooved vapor chamber, *Applied Thermal Engineering*, 29, 2009, 422–430.
- [33] Wang, J.-C., Wang, R.-T., A novel formula for effective thermal conductivity of vapor chamber, *Experimental Techniques*, 35, 2011, 35–40.
- [34] Attia, A. A. A., El-Assal, B. T. A., Experimental investigation of vapor chamber with different working fluids at different charge ratios, *Ain Shams Engineering Journal*, 3, 2012, 289–297.
- [35] Peng, H., Li, J., Ling, X., Study on heat transfer performance of an aluminum flat plate heat pipe with fins in vapor chamber, *Energy Conversion and Management*, 74, 2013, 44–50.
- [36] Naphon, P., Wiriyasart, S., Wongwiset, S., Thermal cooling enhancement techniques for electronic components, *International Communications in Heat and Mass Transfer*, 61, 2015, 140–145.
- [37] Liu, Y., Han, X., Shen, C., Yao, F., Zhang, M., Experimental Study on the Evaporation and Condensation Heat Transfer Characteristics of a Vapor Chamber, *Energies*, 12, 2019, 11.
- [38] Ladekar, C., Pise, A., Nukulwar, M., Lingayat, A., Comparative analysis of integrated heat sink vapor chamber with conventional heat sink for LED cooling, *Materials Today: Proceedings*, 72, 2023, 1136–1142.
- [39] Cengel, Y., Cimbala, J.M., Turner, R.H., *Fundamentals of Thermal-Fluid Science*, Fifth edition, MC Grow Hill, New York, 2003.
- [40] Moffat, R.J., Describing the uncertainties in experimental results, *Experimental Thermal and Fluid Science*, 1988, 3–17.
- [41] Al-Rahman, M.A., Ibrahim, S.A.A., Ahmed, S., Elrifai, M.E., Thermo-hydraulic Characteristic Study of The Flat Plate-Finned Heat Sink, *Journal of Al-Azhar University Engineering Sector*, 2023, (Accepted for publication).

ORCID iD

Mohammed A. Al-Rahman  <https://orcid.org/0000-0002-3687-5744>

Saeed A.A. Ibrahim  <https://orcid.org/0000-0002-8815-4746>

M. Elfaisal Elrefaie  <https://orcid.org/0009-0001-7905-7549>



© 2023 Shahid Chamran University of Ahvaz, Ahvaz, Iran. This article is an open access article distributed under the terms and conditions of the Creative Commons Attribution-NonCommercial 4.0 International (CC BY-NC 4.0 license) (<http://creativecommons.org/licenses/by-nc/4.0/>).

How to cite this article: Al-Rahman, M.A., Ibrahim S.A.A., Elfaisal Elrefaie M., Thermal Performance Study of Plate-Finned Vapor Chamber Heat Sink, *J. Appl. Comput. Mech.*, 10(2), 2024, 304-316. <https://doi.org/10.22055/jacm.2023.44192.4177>

Publisher's Note Shahid Chamran University of Ahvaz remains neutral with regard to jurisdictional claims in published maps and institutional affiliations.

